

Application of SSM/I satellite data to a hurricane simulation

By SHU-HUA CHEN^{1*}, FRANCOIS VANDENBERGHE², GRANT W. PETTY³ and JAMES F. BRESCH²

¹*Department of Land, Air, and Water Resources, University of California, Davis, USA*

²*National Center for Atmospheric Research, Boulder, Colorado, USA*

³*Department of Atmospheric and Oceanic Sciences, University of Wisconsin, Madison, USA*

(Received 19 February 2002; revised 18 June 2003)

SUMMARY

The impact of Special Sensor Microwave/Imager (SSM/I) data on simulations of hurricane *Danny* is assessed. The assimilation of SSM/I data is found to increase the atmospheric moisture content over the Gulf of Mexico, strengthen the low-level cyclonic circulation, shorten the model spin-up time, and significantly improve the simulation of the storm's intensity. Two different approaches for assimilating SSM/I data, namely assimilating retrieved products and assimilating raw measurements, are further compared. The data-assimilation analyses from these two approaches give different moisture distributions in both the horizontal and vertical directions in the storm's vicinity, which may potentially affect the simulated storm's development; however, the simulated storm intensities are considered comparable for the *Danny* case. From sensitivity tests performed in this study, it is also found that the choice of the observational error variances could be potentially important to the model simulations.

KEYWORDS: Brightness temperature Special Sensor Microwave/Imager Total-column water-vapour Variational data assimilation

1. INTRODUCTION

It is well known that atmospheric moisture is crucial to the evolution of severe weather systems because of its potential to release large amounts of latent heat. Therefore, uncertainties in the initial condition humidity-field of numerical weather prediction models could have a significant impact on weather forecasts. These uncertainties can be reduced through the use of observations in model initialization. The conventional observational network of the World Meteorological Organization (WMO) (e.g., upper-air radiosondes and surface stations) provides moisture observations, but these are mostly distributed over land with soundings usually available only twice a day. This is insufficient to sample the rapidly evolving environment of marine weather systems, such as hurricanes, adequately.

Non-conventional observations, such as satellite data, on the other hand, can provide spatially dense information with high temporal repeatability. There are several satellite instruments that measure atmospheric moisture including the Advanced Microwave Sounding Unit (AMSU-B), a humidity sounder (English *et al.* 1994; Rosenkranz 2001), the High-resolution Infrared Radiation Sounder (HIRS) (McNally and Vesperini 1996; Derber and Wu 1998; Engelen and Stephens 1999; Escoffier *et al.* 2001), the Special Sensor Microwave Water vapour Sounder (SSM/T2) (Engelen and Stephens 1999), and Special Sensor Microwave/Imager (SSM/I). The retrieved moisture profiles from HIRS data have a better impact on the non-cloudy mid- to upper-troposphere (McNally and Vesperini 1996; Engelen and Stephens 1999), while the retrieved moisture from SSM/T2 has a greater impact on the lower troposphere over oceans (Engelen and Stephens 1999). In the present study, we shall focus on the SSM/I, which provides data, at a high density, on moisture in the marine atmosphere over non-precipitating areas.

SSM/I data are difficult to use with numerical weather prediction models because SSM/I measurements are not expressed in terms of model variables. They are, like most satellite data, only indirectly related to model variables through complex physical

* Corresponding author: Department of Land, Air and Water Resources, University of California, Davis, CA 95616-8627, USA. e-mail: shachen@ucdavis.edu

relations. Traditionally, these data were inverted before being ingested in numerical weather prediction models. This approach, however, is not optimal; as, in most cases, the inversion problem is usually mathematically ill-posed and the inversion has to be performed with the help of other sources of information. These additional sources are usually referred to as providing a priori information (Rodgers 1990) and can be various, e.g., climatology, model outputs and sounding database. Depending on the quality of this ancillary information, significant error can be introduced during the inversion procedure. In general, this error is correlated with the data assimilation system's background error. Estimating the resulting cross-correlations is very complex and usually these correlations are ignored. In order to assimilate retrievals, however, such information is not always fully required. Joiner and Dee (2000) showed that even though the retrieval errors cannot be properly accounted for, in the end, results might still be comparable to radiance assimilation. They also noted that, if no prior information is used in the retrieved product, then the errors can be properly used and the assimilation of retrieved products will produce the same results as the assimilation of raw measurements.

Advanced data-assimilation techniques based on one-dimensional (1D-Var) (Phalippou 1996; Gérard and Saunders 1999; Joiner and Rokke 2000), three-dimensional (3D-Var) (Deblonde 1999; Hou *et al.* 2000; Fillion 2002; MacDonald *et al.* 2002), or four-dimensional variational algorithms (4D-Var) (Gerard and Saunders 1999; Xiao *et al.* 2000; Pu and Braun 2001; Zupanski *et al.* 2002) have been used to assimilate different types of data, such as those from the TIROS Operational Vertical Sounder (TOVS) (Joiner and Rokke 2000), from the Global Positioning System (MacDonald *et al.* 2002) as well as precipitation data (Fillion 2002) and SSM/I data. Variational assimilation is able to deal with indirect measurements and therefore avoids the need to estimate the retrieval's error and its correlation with the background error of the data-assimilation system. However, variational assimilation of a specific type of observation requires the estimation of the measurement's observational error and the availability of a so-called observation operator, i.e. a mapping from the model variables onto the observed quantities that are assimilated. It also solves the analysis problem iteratively, which can be costly in computer time.

Algorithmic improvements and continual increases in computer power during the past decade have made variational data assimilation ever more practical. There are, nowadays, two possible ways to assimilate SSM/I observations, namely to assimilate retrieved data (Filiberti *et al.* 1994; Ledvina and Pfaendtner 1995; Hou *et al.* 2000; Xiao *et al.* 2000) or to directly assimilate raw observational information, such as satellite radiances (i.e., brightness temperature; see Mo (1999)). The retrieval approach is computationally cost-efficient. However, the retrievals are typically based on statistically derived linear relationships between SSM/I raw measurements and *in situ* observations. This approach might not be applicable to areas where *in situ* observations are not available, are unreliable, or, in extreme cases, when nonlinearities become non-negligible (Petty and Katsaros 1992). On the other hand, directly assimilating observational information using an observation operator may be slightly more expensive, but is physically based (e.g., through use of a physical observational operator) and reduces the dependence of the result on statistical relationships that may or may not be representative of the region in question. It is, in particular, able to reduce systematic biases sometimes present in retrieved data (Deblonde 1999). For example, Phalippou (1996) pointed out that the total-column water-vapour (V) retrieval-algorithm of Alishouse *et al.* (1990) is biased toward underestimating high V values and, to a lesser extent, overestimating low V values. In between assimilating retrieved data and assimilating raw measurements, a 1D-Var retrieval scheme based on a physical radiative-transfer model was developed

(Phalippou 1996). Gérard and Saunders (1999) used this 1D-Var technique to retrieve SSM/I V , which was then assimilated into a 4D-Var system. So far, direct assimilation of SSM/I brightness temperature has been limited to major operational centres. This is partly because the radiative transfer equation must be solved efficiently and accurately. It also requires adjoint operator-code for the radiative-transfer model. Practically, this means that a longer development time and more computational power are needed to assimilate SSM/I brightness temperatures than retrieved products.

In the past decade, scientists have been using retrieved SSM/I products, such as V (Filiberti *et al.* 1994; Deblonde 1999; Gérard and Saunders 1999; Hou *et al.* 2000; Xiao *et al.* 2000), sea-surface wind (SSW) (Boutin and Etcheto 1996; Yu *et al.* 1997; Wick *et al.* 2000), liquid water, and precipitation rate (Hou *et al.* 2000; Xiao *et al.* 2000), to improve weather analyses and model forecasts/simulations. SSM/I retrievals have also been treated as verification data for validating model performance (V) (Vesperini 1998). The SSM/I V has been applied to numerous data-assimilation studies (Filiberti *et al.* 1994; Wu and Derber 1994; Ledvina and Pfaendtner 1995; Aonashi and Shibata 1996; Deblonde 1999; Gérard and Saunders 1999; Hou *et al.* 2000; Xiao *et al.* 2000), and the results show some improvement of analyses and model simulations/forecasts.

Besides examining the impact of assimilating SSM/I data on hurricane intensity and track simulations, in the present paper we compare the performance of the two different approaches—assimilation of retrieved products and raw measurements—in terms of model simulation accuracy and computational cost. It is worth emphasizing that this study is only a first step towards the operational assimilation of SSM/I data. More studies are required and will be carried out. In section 2, we briefly introduce the concept of the 3D-Var data-assimilation system and describe the assimilated data, while in section 3 we present the radiative-transfer model used in the system and provide the observational-error variances. The description of the numerical model and experimental design is given in section 4. The data assimilation analysis, computational efficiency and model simulation results are discussed in section 5 and concluding remarks are made at the end.

2. VARIATIONAL ASSIMILATION SYSTEM AND ASSIMILATED DATA

(a) *Three-dimensional variational assimilation (3D-Var) system*

The MM5 (Fifth-Generation US National Center for Atmospheric Research (NCAR)/Pennsylvania State University Mesoscale Model version 3 (Grell *et al.* 1994)) 3D-Var is applied in this study; its assimilation system is based on the incremental formulation (Courtier *et al.* 1994). The technical aspects of MM5 3D-Var have been detailed by Barker *et al.* 2003. Briefly, it is a model-space-based multivariate incremental analysis system for measurements of pressure, wind, temperature and relative humidity. Currently, it can assimilate conventional data such as the WMO SYNOP, SHIP, METAR, TEMP, SATEM and SATOB reports and those from the National Oceanic and Atmospheric Administration (NOAA) wind-profiler demonstration-network. The cost function includes a background and an observational term. The observational-error covariance-matrix is assumed to be diagonal. The variances are prescribed for each variable and data source according to the observational-profile error-statistics compiled by the US National Centers for Environmental Prediction (NCEP)*. The SSM/I observational-error covariance-matrix is assumed to be diagonal. In the absence of published information on SSM/I-error spatial-correlations, we have preferred

* <http://wwwt.emc.ncep.noaa.gov/gmb/bkistler/oberr/reanl-obs.html> as on 14 January 2004.

to assume the independence of the data rather than to over-prescribe correlations, which would have lessened the impact of the data in the assimilation process.

Following Lorenc *et al.* 2000, the background-error covariance-matrix was designed so as to project on to vertical modes, allowing for separate definitions of the vertical and horizontal correlation functions. The vertical modes were obtained from the decomposition in empirical orthogonal functions (EOFs) of statistical model-forecast-error profiles. These profiles were generated by application of the US National Meteorological Center (NMC) method to the MM5 real-time system run daily at NCAR on a 30 km grid over the continental USA*. Differences between 24 h minus 12 h forecasts valid daily at 12 UTC were averaged in time and space; so as to produce a mean forecast difference profile valid over the USA on a monthly basis. After projection on to the vertical modes, 3-D fields were normalized by the square root of the expected variance of the relevant vertical mode. These normalized fields were then passed through a series of recursive filters that create the smoothing effect of a convolution with a covariance matrix. In that particular case, a first order (exponential smoother) filter was repeatedly applied. The filter parameter (Lorenc 1992) was set so as to approximate Gaussian structure functions with e-folding distance of about 100 km. These values were subjectively set from our experience with MM5 for surface observations. The basic assumption under the application of the filter is that horizontal model forecast error correlations are supposed to be homogeneous and isotropic (see Fig. 1b).

A weak balance-constraint is applied to the analysis through the choice of the analysis or control variables. In our application, hydrometeors are neglected and the model variables (wind, pressure, temperature and water vapour mixing ratio) are transformed into unbalanced stream-function, velocity potential, unbalanced pressure and relative humidity. This choice of control variables follows Lorenc *et al.* (2000). The choice was motivated by the variables' relative independence, so that correlations between analysis variables can be neglected in the background covariance-matrix. The square root of the background covariance-matrix is used as preconditioning.

SSM/I observations are assimilated by adding a new term in the cost function (J) to the existing background (J_b) and conventional observation (J_{conv}) terms:

$$J(x') = J_b + J_{conv} + J_{SSM/I}.$$

This new term $J_{SSM/I}$ is defined as

$$J_{SSM/I}(x') = \frac{1}{2}(\mathbf{H}x' - y^{oi})^T R^{-1}(\mathbf{H}x' - y^{oi}),$$

where x' is the analysis increment defined by

$$x^a = x^b + x'$$

and x^b is the background state (first guess), x^a the desired analysis and R the covariance matrix of SSM/I observation errors. Since observation errors are assumed uncorrelated, the matrix R is simply diagonal with the SSM/I observation-error variances as elements. In our application, these variances are taken as constant in space and time, but varying with frequency channel. The nonlinear operator \mathbf{H} includes a nonlinear observational operator and linear space-interpolation. This operator \mathbf{H} is the vertical integral of the water vapour (V) and surface wind-speed calculation if retrieved V and sea-surface-wind (SSW) data are assimilated, whereas it is the radiative transfer model (Petty and Katsaros 1992; 1994) if brightness temperatures are assimilated. An innovation vector

* <http://rain.mmm.ucar.edu/mm5> as on 13 January 2004.

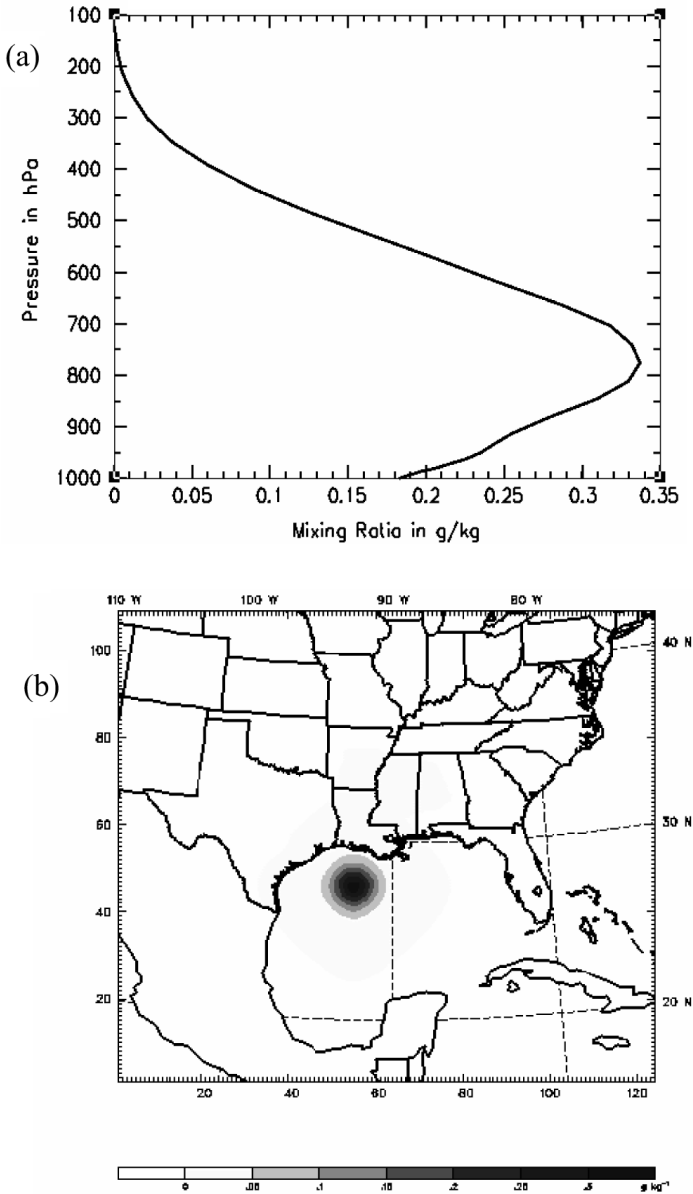


Figure 1. Water-vapour analysis increment (g kg^{-1}) for an assimilation of a single total-column water-vapour (V) observation: (a) vertical profile, and (b) at 775 hPa, the pressure level at which the increment is greatest.

y^{oi} is defined as

$$y^{\text{oi}} = y^{\text{o}} - \mathbf{H}x^{\text{b}},$$

where y^{o} is the observation vector (in the present study, retrieved SSM/I data or SSM/I brightness temperatures).

Under the assumptions that both model-forecast and observational errors are unbiased with Gaussian spatial probability density, white in time and uncorrelated, the 3D-Var solution x^{a} is obtained for the analysis increment x' that minimizes the total cost function. It is, therefore, the model space vector that best fits simultaneously the

background vector and both the conventional and SSM/I observation vectors. This fit is measured by the quadratic distance defined by the background- and observational-error covariance-matrices. The limited-memory quasi-Newton method (Liu and Nocedal 1989) is used to solve the minimization of the cost function.

Assuredly, the assimilation of surface or integral quantities such as SSW and V will be very sensitive to the vertical structure functions that are used in the background-error covariance-matrix. A simple way to visualize these structure functions is to perform single-observation assimilation-experiments (Thépaut *et al.* 1996). As an experiment, we have assimilated a single V -observation at the location of the exemplar for the present investigation, hurricane *Danny*. The observation increment was specified to be 2 kg m^{-2} (2 mm of equivalent precipitable water), the expected observation error. We found that the minimization of the cost function converged in two iterations. The V analysis-increment was increased from 0 to 1.4 kg m^{-2} . Figure 1(a) shows how this integral analysis-increment has been distributed along the vertical profile of water-vapour mixing-ratio. The profile has been projected vertically, using statistical values of forecast error. The maximum increment was found at 775 hPa, corresponding to the maximum of the first eigenvector (not shown) of the model-forecast error. At this pressure altitude, which roughly corresponds to the top of the model's boundary-layer in summer, the forecast error is expected to be the largest. As a consequence, most of the new observational information contained in the integral observation-increment is transferred at that level to correct for deficiencies in the model. Figure 1(b) shows the horizontal water-vapour increment at its maximum (775 hPa). The maximum value of the increment at the site of the observation is about 0.33 g kg^{-1} . The isotropy of the correlation functions can be clearly seen and the decorrelation length can be found where the value of the increment is reduced to e^{-1} of its maximum value, in this case to 0.12 g kg^{-1} . This is the contour level of the second external ring in Fig. 1(b), which stands at about 4 grid points (108 km) from the observation site. Note also, that, through the balance relation, the V observation-increment induces a sub-millimetric wind-circulation (not shown).

(b) *The SSM/I data*

The SSM/I is a conical scanning, four-frequency (19.3 GHz, 22.2 GHz, 37.0 GHz and 85.5 GHz), seven-channel (19H, 22V, 37H, 37V, 85H, and 85V), passive microwave-radiometer, where suffixes H and V indicate horizontal and vertical polarizations respectively, and the corresponding numbers present the integer portion of their frequencies (GHz). The first SSM/I instrument was launched aboard the Defense Meteorological Satellite Program (DMSP) of the US Navy in June 1987. The instrument has a near-constant incidence-angle of 53° ; its mean altitude is approximately 830 km and swath width about 1400 km. The product's resolution is 25 km for V , SSW, and for five channels of brightness temperature (i.e., 19H, 19V, 22V, 37H and 37V), but 12.5 km for brightness temperatures in channels 85H and 85V. Detailed information about the SSM/I instrument was given by Hollinger (1989). The data used in the present study, in each case received from both the DMSP-F13 and DMSP-F14 satellites, are seven-channel brightness temperature, retrieved V and retrieved SSW. These data were obtained from the US National Aeronautics and Space Administration (NASA) Earth Observing System (EOS) data gateway and provided by the Global Hydrology Resource Center at the Global and Hydrology and Climate Center, Huntsville, Alabama, USA. Values of V and SSW were retrieved using the algorithm of Wentz (1993).

(c) *Quality control and data reduction process for SSM/I data*

Data from the SSM/I data undergo several processes before they are used in 3D-Var. Firstly, retrieval of most SSM/I atmospheric parameters is possible only with a low-emissivity background such as the ocean. The microwave emissivity of land and ice surfaces is both high and variable, obscuring changes in brightness-temperature caused by atmospheric absorption and emission. Consequently, SSM/I data referring to points over land and ice are excluded; in the dataset, such points are, instead, marked with a flag indicating the surface property.

Secondly, since the SSM/I data are taken sequentially, only a very few are available at the analysis time. Consequently, in order to assimilate more data, a small time-window is considered for data selection. In particular, since our phenomenon of interest, hurricane *Danny*, changed only slowly, a two-hour time-window (one hour before and one after the initial time) was chosen. For example, the storm moved about 20 km (less than 1 grid interval in domain 2) within two hours. The change in the storm's location and structure was insignificant during this period.

Thirdly, rainfall can contaminate the SSM/I brightness-temperature data and, therefore, an observation-based rain-filter is applied to exclude those rainfall points. In the filter, V and SSW are first retrieved from brightness temperatures using statistical algorithms described by Petty (1994). The retrieved V and SSW are used together with the observed polarization-difference at 37 GHz to retrieve column cloud-liquid-water. When the column cloud-liquid-water is greater than 0.5 mm, the pixel is designated a rainy one and is excluded. Note that points eliminated from the raw data are also excluded from the retrieved data (e.g., using the point's latitude and longitude) before they are assimilated.

Fourthly, a gross-error quality-control is performed to remove observations that differ too much from the model's first guess/background (beyond five times the observation-error variance). The value five is chosen from our experience, given that the first guess is considered reliable.

Lastly, data are reduced so as to decrease the correlation of observations within the same grid box but not across grid boxes. If the data resolution is higher than the model horizontal resolution (81 and 27 km), the reduction takes the average of those valid points which are within the same grid box ('super-obbing'). Consequently, after data reduction, there is at most one observation inside one grid box. Note, however, that other data-reduction processes are possible, such as using the value at the valid point which is closest to the centre of the grid box. Sensitivity tests of the data-reduction process would be interesting, but are not within the main scope of this study.

3. OBSERVATIONAL OPERATOR- AND ERROR-VARIANCES

(a) *SSM/I radiative-transfer model*

Although it is possible to use direct numerical integration of the radiative-transfer equation as the forward model, this method is numerically inefficient. Therefore, we utilize a closed-form analytic approximation to the radiative-transfer equation for microwave observations at SSM/I frequencies. Because the non-precipitating atmosphere is relatively transparent at SSM/I frequencies, brightness temperatures can be expressed with reasonable accuracy as functions of several vertically integrated properties of the atmosphere, such as V , total-column cloud-water and mean cloud-temperature.

Two such analytic models for SSM/I brightness-temperatures are known to the authors: that of Wentz (1992) and that of Petty (Petty 1990; Petty and Katsaros 1992,

1994). Both models are similar in terms of their conceptual basis and potential applications; the main difference is that the Petty model incorporates a more elaborate treatment of the effects of vertical distributions of atmospheric absorbers and of the angular effects of reflection from the wind-roughened ocean surface, whereas the Wentz model uses a single homogeneous slab model for microwave absorption and emission by cloud water, water vapour and oxygen. For the present study, the Petty model was chosen, primarily because it retains a somewhat larger set of environmental input parameters, but also because its coded form was more readily accessible to the authors.

The derivation of the Petty model is discussed by Petty and Katsaros (1992, 1994). Additional partial details concerning empirical calibration and the treatment of ocean surface foam were given by Petty (1990). The model is based on closed-form approximations to the plane-parallel radiative-transfer equation for microwave radiation in a non-scattering atmosphere, assuming exponential profiles of gaseous absorption, a constant lapse-rate, and a geometrically thin absorbing/emitting cloud layer at an arbitrary altitude above the surface. Surface emission/reflection is modelled in the same way as that from a plane dielectric surface, but with theoretical adjustments to account for reflection and emission by wind-induced gravity-waves in the geometric optics limit, plus an empirical model for the effects of foam and capillary waves.

The environmental input-variables for the model are: total-column water-vapour V and water-vapour scale-height H_V , column-cloud liquid-water L , mean cloud-altitude z_L , effective surface-air-temperature T_A , lower-tropospheric lapse-rate Γ , sea surface temperature T_S , surface wind speed U and surface air pressure p_0 . As discussed by Petty (1990), the variables having the strongest effect on microwave brightness temperature at SSM/I frequencies are V , L , and U . All remaining variables impart relatively small (a few K or less) brightness-temperature variations; they are considered as model parameters (Rodgers 1990) and not retrieved from the SSM/I brightness temperature. Note that L is ignored in the 3D-Var system since the initial condition contains no cloud information.

(b) *Nonlinearities in the observational operator*

Because the incremental method is applied in the MM5 3D-Var system, it is necessary to use a tangent linear operator. As a consequence, both tangent linear and adjoint SSM/I operators are developed here, based on the original nonlinear operator. The use of a linearized version instead of the full radiative model is an approximation whose validity will determine how far the solution of the assimilation approximates the true solution. It is, therefore, important to learn about the nonlinear behaviour of the operator, which is much more complicated than other forward operators (i.e., operators for U and V) in this study. A simple test was conducted for this purpose with 6643 sampled atmospheric columns. The base fields and the perturbation fields were put into the tangent linear operator, while their summations were put into the nonlinear operator. Figure 2 shows the relationship of the derived brightness-temperature of the tangent linear operator versus the nonlinear operator for 19 GHz. It clearly shows that the radiative model acts more linearly for vertical polarization than for horizontal polarization. (The same effect was found for 37 GHz and 85 GHz, not shown.) Table 1 gives the root-mean-square (r.m.s.) errors of the tangent linear operator which result from linearization. For each dual-polarization frequency (19 GHz, 37 GHz, and 85 GHz), the r.m.s. error with horizontal polarization is approximately 0.5 K larger than that with vertical polarization. However, these numbers are small enough for us to be confident that the solution will converge.

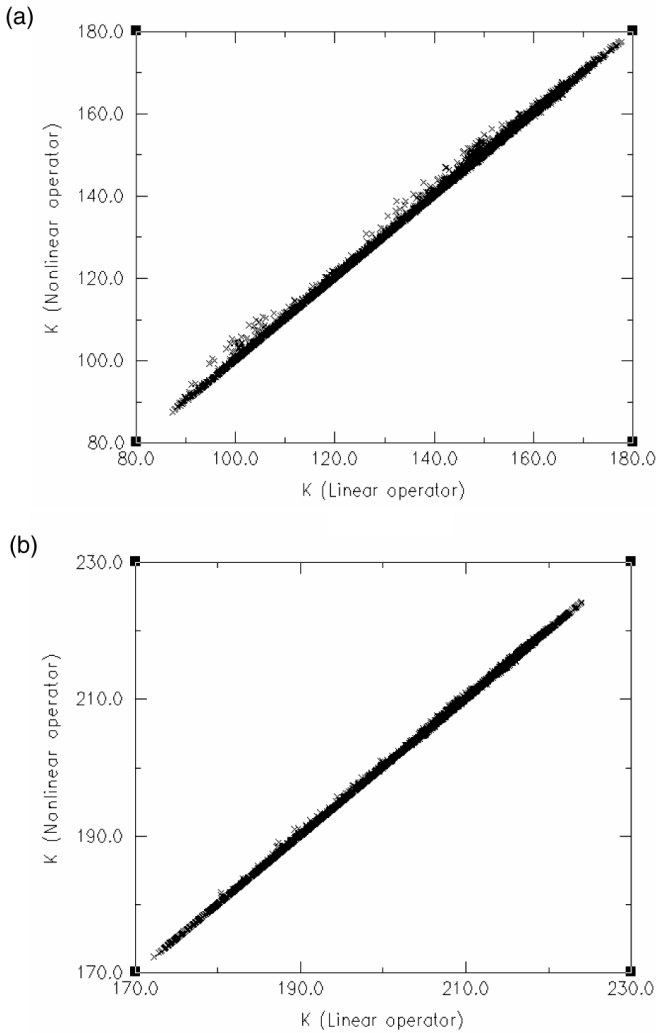


Figure 2. Relationship between derived brightness-temperatures at a frequency of 19 MHz, using a tangent linear operator (x axis) and a nonlinear operator (y axis): (a) horizontal polarization (the channel called 19H in text), and (b) vertical polarization (the channel called 19V in text).

TABLE 1. ROOT MEAN SQUARE (r.m.s.) ERROR OF THE TANGENT LINEAR OPERATOR AS A RESULT OF LINEARIZATION

| | | | | | | | |
|------------------|----------|------------|----------|----------|------------|----------|------------|
| Frequency (GHz) | 19.3 | 19.3 | 22.2 | 37.0 | 37.0 | 85.5 | 85.5 |
| Polarization | vertical | horizontal | vertical | vertical | horizontal | vertical | horizontal |
| SSM/I channel | 19V | 19H | 22V | 37V | 37H | 85V | 85H |
| r.m.s. error (K) | 0.15 | 0.63 | 0.34 | 0.08 | 0.76 | 0.24 | 0.86 |

Note: The total number of sampled atmospheric columns was 6643.

(c) *The observation-error variances*

The observation-error variances required for assimilating brightness temperature are taken to include instrument error (generally less than 1 K for all channels) and representativeness error. Here, the representativeness error comprises both the representation

TABLE 2. VARIANCE OF OBSERVATION ERROR (σ_0^2) FOR EACH SSM/I CHANNEL

| SSM/I channel | 19V | 19H | 22V | 37V | 37H | 85V | 85H |
|--------------------------------|--------------------|--------------------|---------------------|---------------------|---------------------|--------------------|--------------------|
| σ_0^2 (K ²) | (3.0) ² | (3.0) ² | (4.33) ² | (5.65) ² | (5.65) ² | (7.0) ² | (7.0) ² |

error and the parameter error (in the terminology of Rodgers (1990)). It includes, therefore, errors arising from the model's representing a natural continuum as a succession of discrete values, as well as errors caused by parametrizations and approximations in the radiative-transfer model (e.g., lack of spectroscopic data, poor knowledge of ocean surface emissivity and fixed liquid water content). The model's approximations also subsume errors arising from ignorance of the effects of variable beam-filling by inhomogeneous clouds, especially in view of the disparate spatial resolutions of the SSM/I channels (12.5 km at 85 GHz, 25 km at others). The true values of the total-error variance are difficult to estimate and in any case are likely to be scene-dependent. Based on our experience, we have assigned observation-error standard-deviations ranging from 3 K for the 19V channel to 7 K for 85H (Table 2). This value of the standard deviation, 7 K, reflects the expected sensitivity at 85 GHz to cloud inhomogeneities and uncertainties in models of the water-vapour-continuum absorption.

The errors in assimilating SSM/I brightness-temperatures can also come from biases in the observed satellite data. The biases of the SSM/I brightness temperature from satellite F-13, for example, have been estimated by Gérard and Saunders (1999) using a representative set of first-guess fields. These numbers are therefore model dependent. Since it will take a large amount of effort to study the biases of the SSM/I brightness temperature for the MM5 model systematically, we leave this for future study and, in the present work, ignore bias errors.

With a similar retrieval algorithm (Wentz 1993), different numbers for the standard deviation have been used, such as 1.6 m s⁻¹ for SSW by Boutin and Etcheto (1996), 1 kg m⁻² for *V* by Hou *et al.* (2000), and about 4–5 kg m⁻² for *V* by Deblonde (1999). In the present work, the standard deviations for SSW and *V* are assigned as 2.5 m s⁻¹ and 2 kg m⁻² respectively. That for SSW is an estimate provided by the US Air Force Weather Agency which performs SSM/I retrievals daily. Note that after this study, NCEP provided estimates for SSM/I ocean surface wind of 2.2 m s⁻¹. The values of *V* correspond to the accuracy of Global Positioning System (GPS) ground-based measurements, for which many statistical studies and comparison have been performed. This choice for *V* error implicitly assumes that SSM/I data are at least as accurate as GPS *V* measurements. Note that these numbers are for observation errors, i.e. measurement and instrument errors.

4. EXPERIMENT DESIGN

(a) *Hurricane Danny*

Hurricane Danny came from a pre-existing, non-tropical, weather system: a cluster of thunderstorms, which originated over the south-eastern USA on 13 July 1997. The system drifted southward to the Gulf of Mexico and contributed to the formation of a small weak depression in the lower troposphere on the 14th. The system became a better-organized tropical depression at 1200 UTC 16 July; 27 hours later it was classed as a tropical storm with a central pressure of 1007 hPa and a maximum wind of 45 knots (23 m s⁻¹). At 0000 UTC 18 July, the central pressure had fallen to 997 hPa and the wind increased to 50 knots (26 m s⁻¹). The storm was classified as a hurricane at 0700 UTC 18 July with a central pressure of 992 hPa and a maximum wind of 65 knots (33 m s⁻¹).

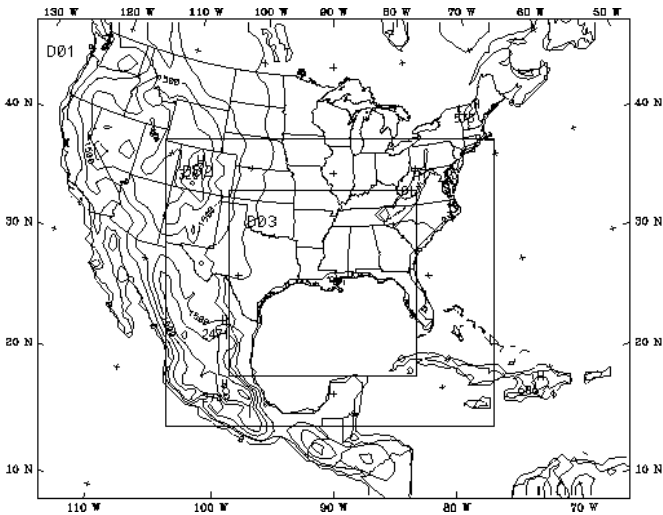


Figure 3. Three nested domains used in MM5 model simulations. The terrain corresponds to the outer domain, domain 1. Resolutions are: domain 1, 81 km; domain 2, 27 km, and domain 3, 9 km.

The pressure reached its minimum (984 hPa) at 0000 UTC 19 July. Seventeen hours later it was slowly filling over the south-eastern USA. *Danny* drifted very slowly until 23 July, and, overall, moved in an east-north-east direction. We shall focus on its early period, when it was intensifying in the Gulf of Mexico.

In the official forecasts for *Danny*, the average track errors were about 83 km at 12 h, 189 km at 24 h, 258 km at 36 h, and 278 km at 48 h. A bias to the left in the forecasts was reported when *Danny* was in the Gulf of Mexico (NCEP 1997). As will be shown later, the simulations in the present work also show a bias to the left of the observed track.

(b) Experiments

MM5 with two-way nest interaction is used for all simulations. Figure 3 shows the three domains (81 km, 27 km and 9 km) superimposed with the terrain of domain 1. Half of domain 3 covers the Gulf of Mexico, where the hurricane formed and developed. The grid dimensions are $75 \times 61 \times 30$, $124 \times 109 \times 30$, and $211 \times 211 \times 30$ in the x , y and z directions in domains 1, 2, and 3 respectively. The grids cover three embedded geographical regions of about $5994 \text{ km} \times 4860 \text{ km}$, $3321 \text{ km} \times 2916 \text{ km}$ and $1890 \text{ km} \times 1890 \text{ km}$. Vertically, the model extends from the surface up to 100 hPa. Only domains 1 and 2 are initialized with analysis data; the initial conditions of domain 3 are interpolated from those of domain 2. The Betts–Miller cumulus scheme (Betts 1986; Betts and Miller 1986; Janjic 1994), Blackadar boundary-layer scheme (Blackadar 1979), mixed-phase microphysics, and cloud-radiation schemes are activated. For each simulation, MM5 integrates 48 hours with a time step of 240 seconds in domain 1.

The model starts integrating at 0000 UTC 17 July 1997 for 48 hours with different initial conditions as indicated in Table 3 (analysis with or without 3D-Var). Two data sets are used in the assimilation: SSM/I brightness-temperatures and SSM/I retrieved data. Note that only SSM/I data are used as observations (no conventional data are used). The SSM/I retrievals obtained from NASA EOS were derived using Wentz's (1993) algorithm. Figure 4 shows the area covered by the SSM/I data which were used (both retrieved data and brightness temperatures are from the same areas) within a two-hour

TABLE 3. CHARACTERISTICS OF THE NUMERICAL EXPERIMENTS WITH DIFFERENT INITIAL CONDITIONS

| Case | Assimilated data | Special characteristics |
|---------|------------------|---|
| CONTROL | None | |
| RV | V and SSW | $\sigma_o^2(V) = 4 \text{ mm}^2$; $\sigma_o^2(\text{SSW}) = 6.25 \text{ m}^2\text{s}^{-2}$ |
| TB | T_b | |
| RVS | V and SSW | $\sigma_o^2(V) = 16 \text{ mm}^2$; $\sigma_o^2(\text{SSW}) = 25 \text{ m}^2\text{s}^{-2}$ |
| TBS | T_b | $\sigma_o^2 = 9 \text{ K}^2$ for each channel |

RV denotes assimilation based on retrieved values.

V denotes SSM/I retrieved total-column water-vapour.

SSW denotes SSM/I retrieved sea surface wind.

σ_o^2 denotes variance of the observation-error.

TB denotes assimilation based on brightness temperature.

T_b denotes SSM/I brightness temperature.

RVS denotes sensitivity test identical to RV, except that the standard deviation of the observation error of RVS is twice that of RV.

TBS denotes sensitivity test identical to TB, but with a constant standard deviation of the observation error for each channel.

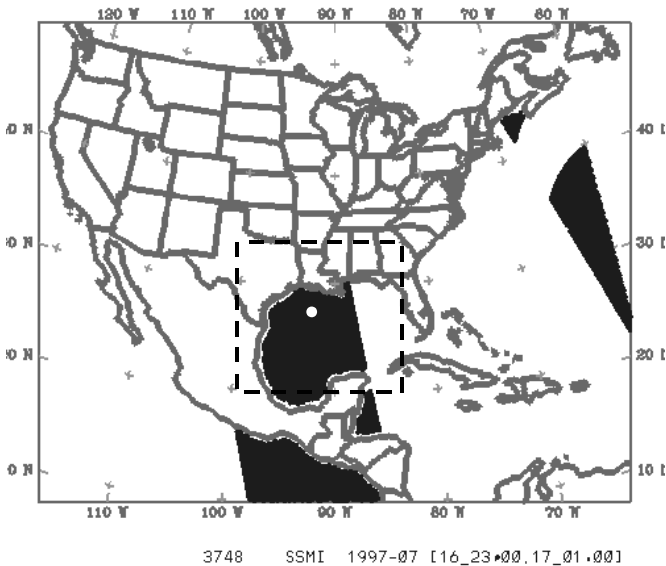


Figure 4. Coverage of SSM/I data used in 3D-Var during the two-hour time-window (23 UTC 16 July 1997 to 01 UTC 17 July 1997): data swaths are shaded. The white dot in the Gulf of Mexico shows the position of the centre of the tropical depression at 00 UTC, 17 July 1997.

time-window (2300 UTC 16 July–0100 UTC 17 July). There is one swath, from satellite F-13, which passes exactly over the initial location of the hurricane (white dot in Fig. 4). *Danny* was then about 200 km from the coast. At this time, the system was weak and the precipitation probably not too intense. As a consequence, the proportion of SSM/I data excluded because of rain contamination is close to its minimum. Though the system is close to the coast, the storm centre is far enough from land for SSM/I data to be available over it, and the southern part of the system is fully covered. The NCEP Global Data Assimilation System (GDAS) data (with 2.5 latitude degrees by 2.5 longitude degrees resolution) are used for the boundary conditions, and for the model's initial conditions (in the CONTROL case) or the first guess/background of the 3D-Var (in the other cases). CONTROL is the only case which does not use any SSM/I data and is used here mainly

for purposes of comparison. Two other cases, RV and TB (which assimilate SSM/I retrieved-data and brightness-temperatures respectively), are used to evaluate the impact of the SSM/I data on hurricane simulations, and also to compare these two different approaches. Two sensitivity tests, denoted by RVS and TBS, were also carried out to examine the influence of different observation-error variances. The RVS experiment is identical to the RV case, except that the observation-error standard-deviations are twice the values used in RV. TBS uses a constant observation-error variance ($\sigma_0^2 = 9 \text{ K}^2$) for every channel, whilst TB uses the numbers shown in Table 2. (Assimilation experiments with conventional data had been performed beforehand. Their impact was found to be almost nil, which was not surprising given the coarse resolution of the sounding network on the coast. Consequently, and because we wanted primarily to study the impact of SSM/I, we decided not to use conventional data. We also considered that an isolated study of SSM/I would help us understand the performance of the data. However, we also noted that the NCEP GDAS model used to initialize the domain of the mesoscale model had already assimilated the conventional observations: they were already in the first guess of our 3D-Var simulations.)

5. DISCUSSION

(a) *Initial conditions*

Figure 5 shows the initial condition (first guess for 3D-Var) over either domain 2 or a portion of domain 2 (dashed box in Fig. 4) for the CONTROL case. There is a weak cyclonic circulation with a low-pressure centre of 1013 hPa (Fig. 5(a)) over the north-west Gulf of Mexico, which is the initial location of the hurricane (black dot in Fig. 5(a)). A moist tongue extends from the land south-westward to near the storm centre over the northern Gulf (Fig. 5(b)), coincident with the storm's path during previous days when the system drifted from the land to the Gulf. The low-pressure centre was tilted up to 500 hPa, with a warm core in the middle troposphere (Fig. 5(c)). The upper portion of the storm is semi-embedded inside a short-wave upper-level trough (Fig. 5(d)). Compared with the major wave downstream, this short wave is surrounded by much weaker flow, which may be one reason why the storm moved slowly during its early stages.

Figure 6(a) shows the differences from the first guess (or CONTROL case) of the vertical integral of water vapour, V , and 950 hPa wind vectors, for the RV case, at the initial time (00 UTC 17 July 1997) in domain 2. Figure 6(b) shows the corresponding differences for the TB case. A cyclonic circulation anomaly, which increases low-level convergence, was obtained after assimilating SSM/I data, whether the retrieved data or brightness temperatures. Both wind deviation patterns are very similar, with the strongest anomalies surrounding the storm, a northerly anomalous flow to the west of the storm centre, a weaker southerly anomalous flow east of the storm, and a north-easterly anomalous flow over the south-west Gulf of Mexico. However, the cyclonic circulation when the assimilated data are 'retrieved' (8.6 m s^{-1} maximum wind increment) is stronger than when they are brightness temperatures (3.2 m s^{-1}).

Although the two assimilation methods produce similar wind differences from the CONTROL analysis, differences in the V fields (Figs. 6(a) and (b)) are more substantial. Note that the V field from the CONTROL case (not shown) has a pattern similar to the water-vapour mixing ratio field shown in Fig. 5(b). Figures 6(a) and (b) show that the assimilated SSM/I data added moisture near the storm centre and over most other parts of the Gulf, but that the two methods moistened the air around the storm in quite different ways. The increments for the RV case (Fig. 6(a)) are smoother with a maximum south-southwest of the storm centre, whereas those for the TB case (Fig. 6(b)) are more

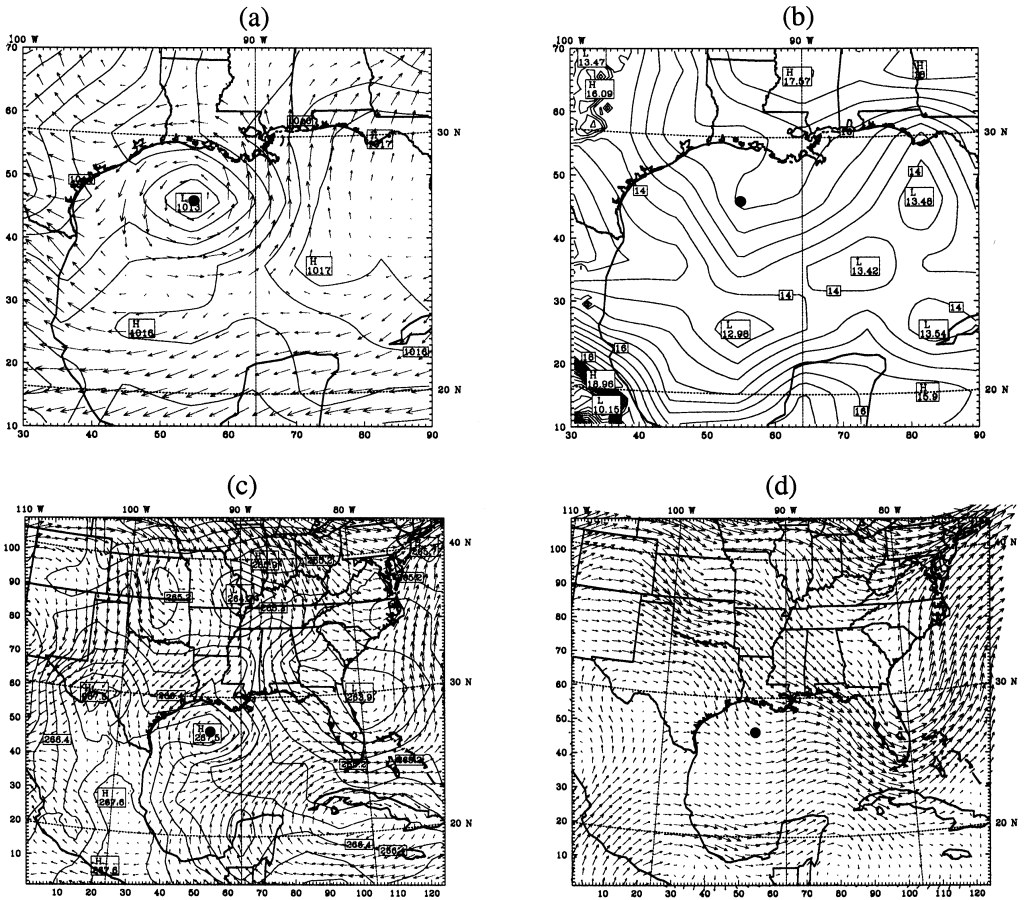


Figure 5. CONTROL case, 00 UTC 17 July 1997: (a) sea-level pressure (SLP) (isobars at 0.5 hPa intervals) and 950 hPa wind vectors; (b) 950 hPa water-vapour mixing-ratio (contours at 0.5 g kg^{-1} intervals); (c) 500 hPa temperature (isotherms at 0.3 K intervals) and wind vectors, and (d) 300 hPa wind vectors. The black dot in the Gulf of Mexico shows the position of the centre of the tropical depression. Panels (a) and (b) are for the box shown by a dashed line in Fig. 4. Panels (c) and (d) are for domain 2, see Fig. 3. The length of the longest arrow in each of the three panels (a), (c) and (d) denotes the same wind strength.

complex and give a stronger maximum SE of the storm. The increments over most of the rest of the Gulf of Mexico for both these cases show similarities, such as the moist band from the storm centre to the central and south-western part of the Gulf, but slightly different magnitudes. Figure 7 shows the ‘innovation’ (observation minus first-guess) of V and sea-surface wind-speed (the observations contain no direction information) for the RV case. As expected, the increment in Fig. 6(a) matches the innovation quite well: positive increments with a local maximum of V are located in the SW Gulf, where Fig. 7 shows smaller values of innovation without a local maximum. However, surface wind speed has a local maximum there, and it may be that it is the use of the multivariate incremental method which has led to a consequential local maximum of V .

Figure 8(a) shows the relationship of the values of V derived from the RV and TB analyses within part of the Gulf (all points within the rectangular box from point (45, 10) to point (80, 53) in domain 2), while Fig. 8(b) shows how the difference in the values of V derived in these two analyses (TB – RV) varies with the value of V

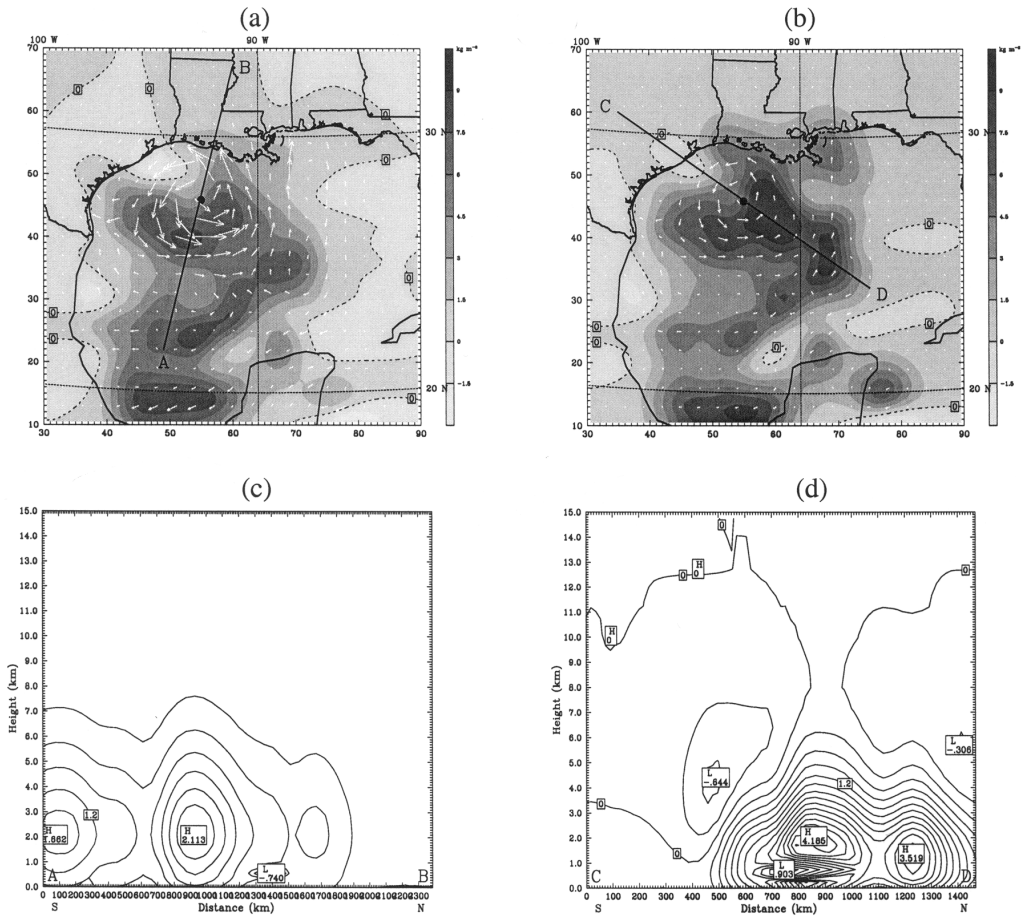


Figure 6. Differences at 00 UTC 17 July 1997: (a) between the RV and CONTROL cases of the vertical integration of water vapour (kg m^{-2}) and 950 hPa wind vector; (b) as (a) but between the TB and CONTROL cases; (c) vertical cross-section of water-vapour mixing-ratio (g kg^{-1}) along the line AB in (a), and (d) as (c) but along the line CD in (b). In (c) and (d), the contour interval is 0.3 g kg^{-1} and the height ranges linearly from mean sea level to 15 km.

from the TB analysis. When V is less than 37 kg m^{-2} , both analyses give very similar results. However, points begin to scatter as V exceeds about 37 kg m^{-2} . Differences between the TB and RV approaches increase for $V > 40 \text{ kg m}^{-2}$ (Fig. 8(b)) and can reach 5 kg m^{-2} , about 2.5 times the assumed standard deviation of the observation error of V ($\sigma_0 = 2 \text{ mm}$). Differences in V are greatest for high values of V . This may be because errors in model parameters have been underestimated and/or because cloud liquid water in the radiative transfer model has been ignored. (The total errors would be about 2 K for each channel in the present study.) We intend to do further work in this direction. Note that most of the large differences are in the important region in the immediate vicinity of the storm, where the largest increments tend to be located (Figs. 6(a) and (b)).

The 3D-Var analysis for the TBS case (not shown) is very similar to that for the TB case, with slight differences in fine structures. Maximum and minimum local values of V are both more extreme in the TBS case than in the TB case. The maximum surface-wind increment (difference from the CONTROL case) is 5.2 m s^{-1} for the TBS case

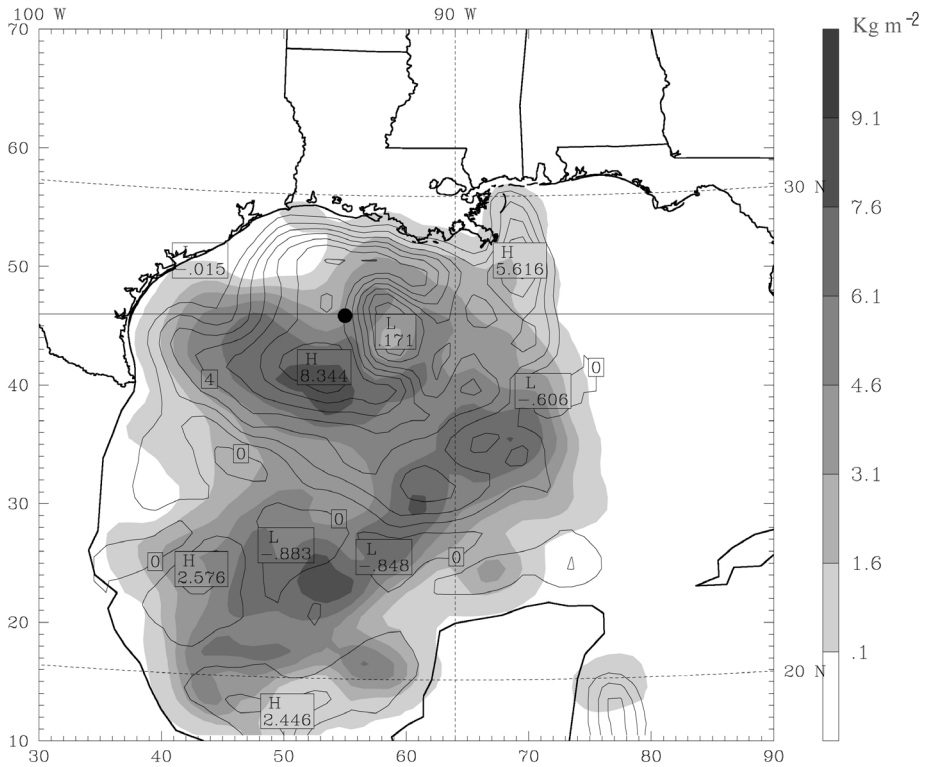


Figure 7. 'Innovation' (difference between observed and first-guess fields) of total-column water-vapour (V) (stippling) and sea-surface wind-speed (isotachs at 1 m s^{-1} intervals) from the RV case.

(3.2 m s^{-1} for the TB case). The 3D-Var analyses for the RV and RVS cases are also quite similar. The difference of the maximum V between these two cases can reach 2.51 kg m^{-2} , and the maximum surface wind increment is 3.9 m s^{-1} for the RVS case (8.6 m s^{-1} for the RV case).

Figures 6(c) and (d) show vertical cross-sections of water-vapour increment passing through the storm centre and the local maximum of V increment in Figs. 6(a) (along line AB) and 6(b) (along line CD), respectively. These two sections, at different angles through the centre of the storm, show quite different patterns of moisture increment. The pattern in the SSW/NNE section for the RV case (Fig. 6(c)) is nearly elliptical, and the three local maxima are at about the same height. For the TB case, on the other hand, the pattern of the water-vapour increment in the NW/SE section shown in Fig. 6(d) has much stronger gradients in both the horizontal and vertical. It is wavier than in the RV case and the heights of the local maxima are slightly different. Different vertical cross-sections of the same quantities from the RV and TB cases around the storm are similar but are not shown. Both assimilations tend to cool the storm centre at lower levels (not shown). (The magnitudes of the increments at upper levels are also much smaller). The vertical cross-sections of moisture and 950 hPa wind vectors from the RVS (TBS) case are again similar to those from the RV (TB) case, with differences in fine structure.

(b) Computational costs of the data assimilation

When satellite data are being assimilated directly, as at operational numerical weather prediction centres, not only is developing an adjoint model and/or a linear

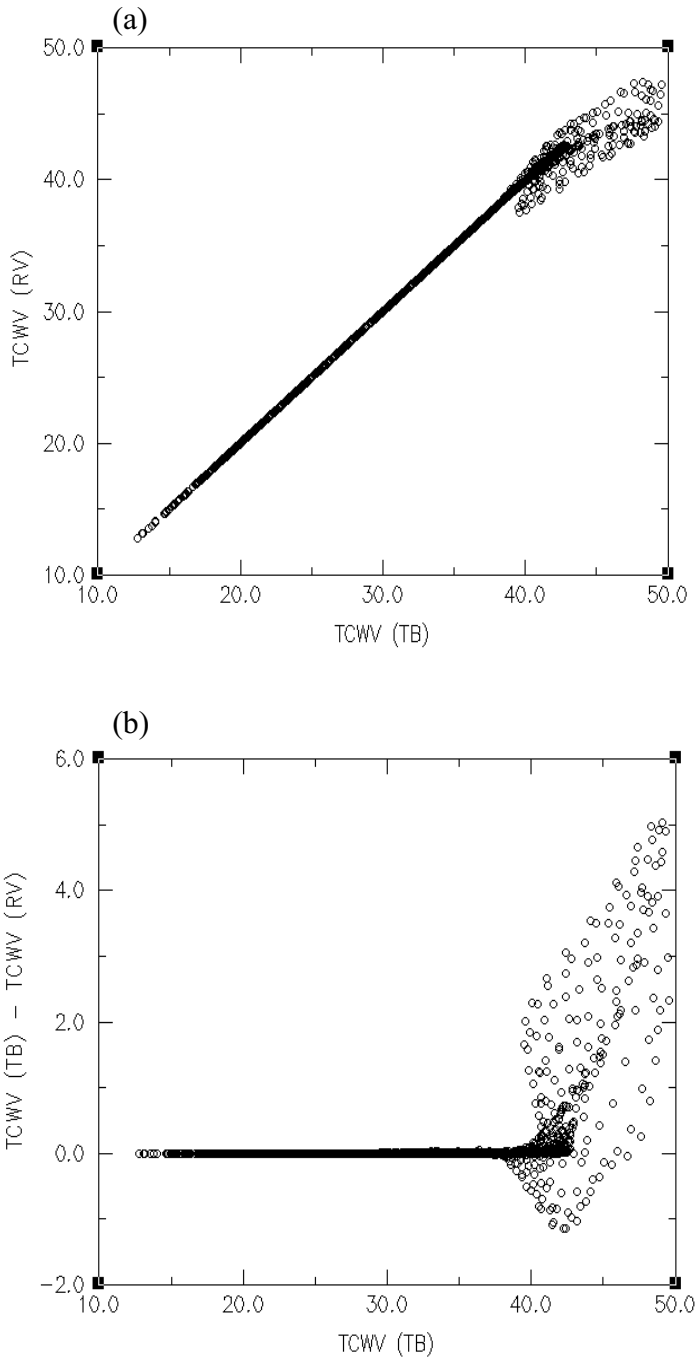


Figure 8. Total-column water-vapour (V) (kg m^{-2}) within part of the Gulf of Mexico (all points within the rectangular box from point (45, 10) to point (80, 53) in domain 2, see Figs. 3 and 5): (a) from the analyses assimilating retrieved data (RV) and brightness temperatures (TB), and (b) variation of difference in V derived in the two analyses (TB-RV) with the value in the TB analysis.

TABLE 4. NUMBER OF ITERATIONS AND COMPUTER CPU TIME NEEDED TO COMPUTE DOMAIN 1 AND DOMAIN 2

| Case | Domain 1 | | Domain 2 | |
|------|-------------------|---------------------------|-------------------|---------------------------|
| | No. of iterations | 3D-Var CPU time (minutes) | No. of iterations | 3D-Var CPU time (minutes) |
| RV | 18 | 0.56 | 18 | 1.64 |
| TB | 22 | 0.97 | 25 | 3.46 |
| RVS | 11 | 0.39 | 11 | 1.05 |
| TBS | 19 | 0.86 | 21 | 2.72 |

Figure 3 shows the area covered by each domain. See Table 3 for expansions of RV, TB, RVS and TBS.

model complex but also computational time is a major concern. Table 4 shows the number of iterations and the total computer central processing unit (CPU) time required for 3D-Var for each experiment. In the present work, all the 3D-Var calculations were performed on a single-processor Compaq Alpha ES40 machine. The MM5 model was integrated on a hybrid-memory IBM parallel machine using 4 nodes with 4 processors per node. The TB case requires about twice as much CPU time as the RV case and about four-thirds as many iterations. Compared to the total CPU time spent on a 48 hour model integration (which is about 157 hours) the CPU time for data assimilation in the TB case (3.46 minutes) is negligible. Although different machines were used here, this conclusion should also be valid if both tasks use the same type of machine. It is true that the ratio of data-assimilation time to model-integration time will get larger as more data types are assimilated. The CPU time should still be affordable for directly assimilating observed information with 3D-Var, especially since computer resources are still rapidly increasing.

(c) *Simulation results*

In this study, we assess the impact of SSM/I data on hurricane simulations and evaluate two different assimilating approaches in a very simple fashion—by comparing the model simulations with the observed storm track and (best-track) sea-level-pressure (SLP) at the storm centre. Furthermore, the cloud coverage from satellite imagery is qualitatively compared with those derived from model simulation results. Figure 9(a) shows the evolution of the observed and modelled storm central SLP. The observed SLP was 1011.5 hPa at 0000 UTC 17 July and dropped to 984 hPa after 48 hours (line O in Fig. 9(a)); the rate of fall of the SLP remains nearly constant for the first 36 hours and then slightly decreases from 36 to 48 hours. At the initial time, the SLPs for all experiments are slightly higher than the observed (1013 hPa for the CONTROL case and 1013.5 hPa for the others). For the CONTROL case (line C), the pressure decreased slightly during the first 24 hours, and then slowly fell more steeply to 1003.5 hPa by 48-h, 19.5 hPa above the observed value. The SLP from the RV case (line R) closely matches observations for the first 24-h; however, the rate of fall increases after 24 hours and, by the end of the simulation reaches 976 hPa, 8 hPa below that observed. For the TB case (line T), the simulated SLP is the same as the RV case for the first 24 hours, falls faster between 24 and 36 hours and then more slowly after 36 hours, finally reaching 983 hPa (1 hPa deeper than observed). Note that during the final 12 hours the observed SLP deepens 5 hPa, but 12 hPa in the RV case and 3 hPa in the TB case. The SLP in the RVS case drops more slowly than that in the TBS, whose rate of fall is the same as those from the TB and RV cases during the first 24 hours. From 24 to 36 hours, both the RVS and TBS fall faster than the other cases (i.e. RV and TB cases), with the RVS case falling fastest. During the final 12 hours, their falls slow down, as was observed. The SLP for

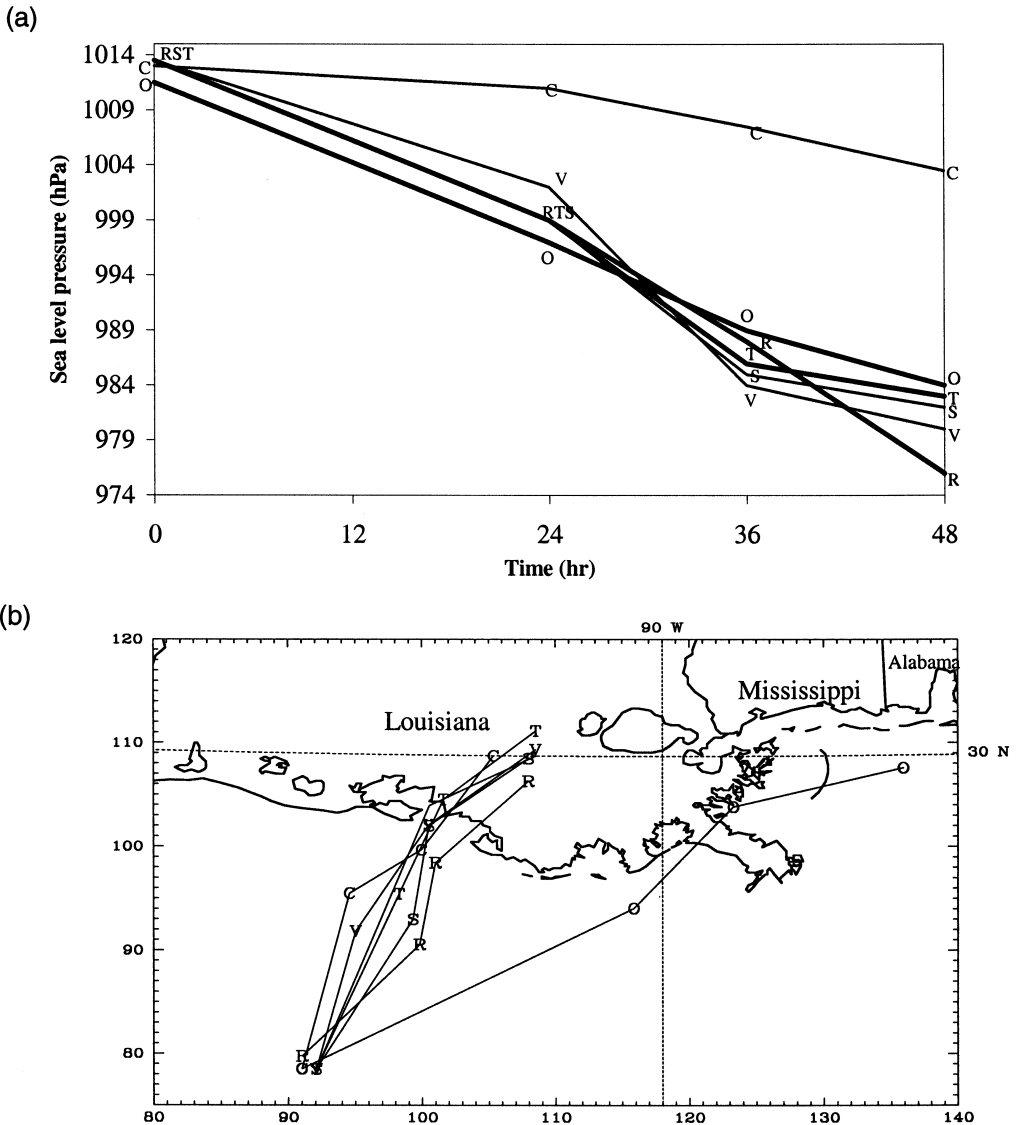


Figure 9. The observed storm (O) during the 48 hour period ending 00 UTC 19 July 1997 and simulated using five different initial conditions, as indicated in Table 3, for part of domain 3 (see Fig. 3) (CONTROL (C), assimilation of retrieved data (RV) (R), assimilation of brightness temperature (TB) (T) and sensitivity tests for retrieved data (RVS) (V) and brightness temperature (TBS) (S)): (a) sea level pressure (hPa) at storm centre, and (b) track of storm centre.

the RVS case is about 4 hPa below that observed, while the TBS case is 2 hPa below that observed at the end of simulation. In this study, the results show that the use of different observation-error variances affects the model simulation, in particular during the final 12 hours, although it is hard to conclude that one is superior to the others. More studies are required in order to get optimized observation-error variances for both brightness temperature and retrieved data.

Figures 10(a) and (b) show the first 6 h accumulated rainfall from the RV and TB cases respectively. The location of the maximum rainfall and the precipitation patterns

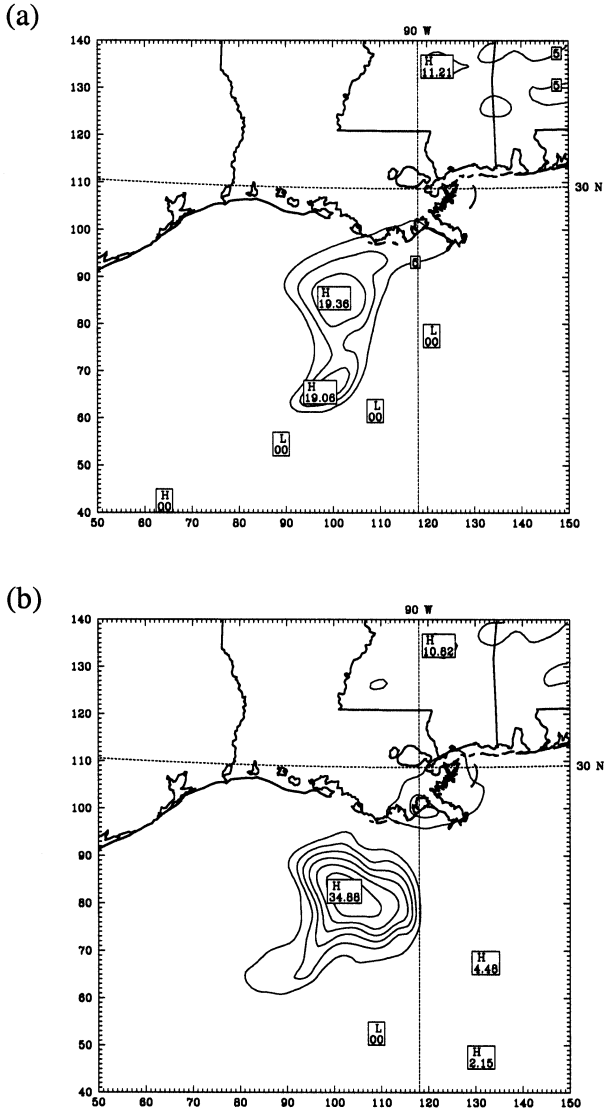


Figure 10. Accumulated rainfall during the first six hours of two simulations (contour interval 5 mm) based on assimilation of: (a) retrieved values (RV) and (b) brightness temperature (TB).

TABLE 5. TRACK ERRORS IN MODEL SIMULATIONS

| Case | Error after 24 hours (km) | Error after 36 hours (km) | Error after 48 hours (km) |
|--------------------|---------------------------|---------------------------|---------------------------|
| CONTROL | 195 | 217 | 280 |
| RV | 150 | 210 | 256 |
| TB | 162 | 198 | 252 |
| RVS | 191 | 209 | 251 |
| TBS | 152 | 209 | 255 |
| Official forecasts | 189 | 258 | 278 |

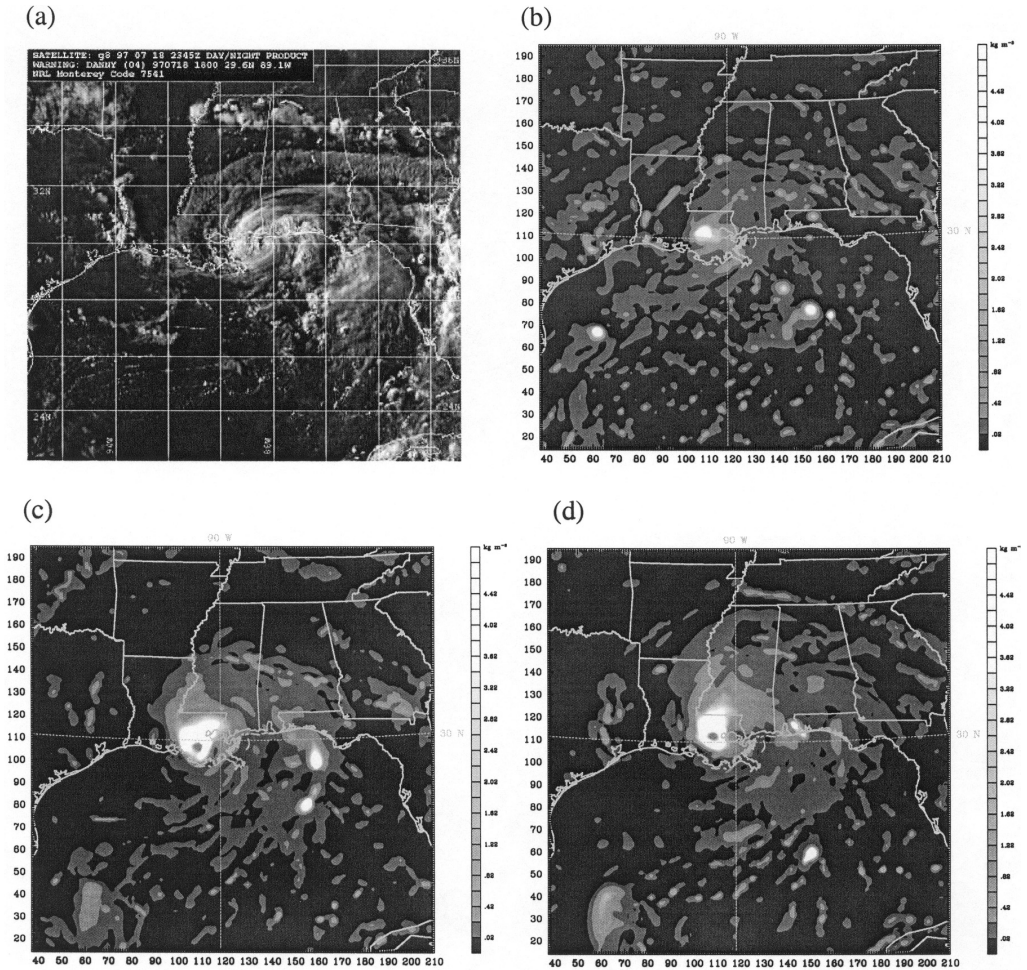


Figure 11. Images of the storm at about 1800 local time 18 July 1997: (a) GOES-8 2345 UTC 18 July (courtesy US Naval Research Laboratory); (b) vertical integration of cloud water, ice, rain and snow (kg m^{-2}) for CONTROL case at 00 UTC 19 July; (c) as (b) but for assimilated retrieved values (RV) case; (d) as (b) but for assimilated brightness temperature (TB) case.

in the storm's vicinity, as well as in the coastal regions, differ between the two cases. On the other hand, both experiments give similar rainfall patterns over inland areas. The storm in the RV and TB cases starts producing light rainfall after two and one hours of simulation, respectively, while it takes at least 8 hours to produce precipitation in the CONTROL case. When SSM/I data are assimilated, MM5 does not need, or needs much less, spin-up time and is able to maintain the cyclone's central pressure and capture its deepening rate.

Figure 9(b) shows the tracks of the observed and modelled cyclones over part of domain 3. Compared with the impact on simulated storm intensity of assimilating SSM/I data, its improvement in simulating storm track is quite small. The observed hurricane passed through the north-west Mississippi River delta and reached the coastal areas of southern Mississippi and Alabama, while all the model-simulated hurricanes tracked toward inland Louisiana. Assimilating SSM/I data reduces the track errors (as compared to CONTROL): all cases exhibit slight improvements over the official

forecasts (Table 5). However, all cases tend to bias the track to the left as did the official forecasts. This might indicate that the prevailing wind in the middle to upper levels is not accurate enough in the initial condition (NCEP GDAS).

Figure 11(a) shows a satellite image (2345 UTC 18 July 1997) and Figs. 11(b), (c) and (d) cloud patterns derived from vertical integration of model hydrometeors at 0000 UTC 19 July 1997 for the CONTROL, RV, and TB cases respectively. Only a qualitative comparison is made here. The hurricane in the satellite image (Fig. 11(a)) has a well-defined structure, with features, such as eye, eye wall, spiral cloud bands and deep convection surrounding the hurricane eye, all clearly visible. Deep convection is also noted along the east boundary of the plotted domain over Florida. For the CONTROL case (Fig. 11(b)), the hurricane is not well developed (1003.5 hPa SLP at the storm centre), and there is no eye. Compared with the CONTROL case, the RV and TB cases (Figs. 11(c) and (d)) produce much better-organized storms, including a hurricane eye, eye wall and some cloud-band structure. However, neither of them captures the observed cloud bands well, such as the band from southwest Mississippi through central Alabama to central Georgia and the other one from the west edge of Florida that extended southwestward into the Gulf. However, these cloud bands may be mostly cirrus which, while showing up in the image, do not contribute much water to the integrated values shown in Figs. 11(b), (c), and (d). The models also fail to simulate the deep convection along the eastern boundary of the plotted domain over Florida, and none of them simulates the correct track—all have a leftward bias.

6. CONCLUDING REMARKS

Based on the results from the 3D-Var and model simulations performed in this study, we have learned that the NCEP GDAS analyses did not have enough moisture over the Gulf of Mexico and the initial circulation at the low levels was not strong enough. This could be the result of the coarse resolution of the NCEP GDAS data, a lack of moisture observations in the vicinity of the storm, or an ineffective bogussing scheme, as the sea level pressure (SLP) at the storm centre was under-estimated by about 20 hPa after a 48 hour simulation (CONTROL case). Assimilating SSM/I data not only increased the moisture content over most of the Gulf of Mexico, but also strengthened the low-level cyclonic circulation, giving a better convergence field and reduced model spin-up time. Moreover, compared to the CONTROL case, the intensity of the simulated hurricane was significantly improved and its structure much better organized. We conclude, therefore, that, in this case study, assimilating SSM/I data (either retrieved data or brightness temperatures) had a strong positive impact on hurricane simulations. On the other hand, the 3D-Var analyses from the RV case (assimilating retrieved SSM/I data) and from the TB case (assimilating SSM/I brightness temperatures) gave notable discrepancies. However, based on the model simulation results for this single storm, neither of the cases stands out as superior to the other.

Two important facts also emerge. Firstly, the sensitivity study shows that for the same frequency, the mathematical operator we used has a better linearity for the vertical polarization channel than for the horizontal one. (Though the result also shows that the linear approximation for every channel is fairly reasonable (small r.m.s. errors), and therefore the solution is expected to converge.) Secondly, the model simulations initialized by assimilating SSM/I data are still sensitive to the given observation-error variances. For example, during the final 12 hours of the simulations, the rate of fall of SLP at the centre of the storm calculated from the TB, RVS and TBS reduced, as it does in the definitive operational analysis, but it did not do so in the RV case.

This study presents a very preliminary result for comparing the RV and TB approaches. To produce a more general conclusion, more case studies, especially extreme cases, and more sensitivity tests of observational error variances for both retrieved data and brightness temperatures will be required.

The official track forecasts from the Tropical Prediction Center showed a left bias, while a consistent left bias is also found in our simulations for hurricane *Danny*. This indicates that the initial steering wind in the middle to upper troposphere, which is important to the model track simulations/forecasts, may not have been accurate enough. Although the tracks are also slightly improved after taking into account SSM/I data, we understand that the SSM/I data are unable to provide enough prevailing wind information through three-dimensional data assimilation. To compensate for the shortcomings of the SSM/I data, extra information from other types of instruments, such as lidar, might be needed. We also made no use of SSM/I liquid-water measurement (although its error was considered), and we leave this for future work.

ACKNOWLEDGEMENTS

The authors would like to thank the MM5 3D-Var group, especially D. Barker, Y.-R. Guo and W. Huang. Further thanks are given to S. Low-Nam, H.-C. Lin, W. Wang, J. Powers and Sherry Harrison for their help, and to the editor and two anonymous reviewers for their comments. The SSM/I data were provided by the Global Hydrology Resource Center at the Global Hydrology and Climate Center, NASA, Huntsville, Alabama. The computing resources of the IBM parallel machines were provided by NCAR under SCD Junior Faculty Grant 36131024, and the 3D-Var analyses were performed on Compaq Alpha machines supplied under a joint External Technology Grant between Compaq, iMSC Corporation and UCAR. This work was originally supported by the US Air Force Weather Agency.

REFERENCES

- Alishouse, J. C., Snyder, S. A., Vongsathorn, J. and Ferraro, R. R. 1990 Determination of oceanic total precipitable water from the SSM/I. *IEEE Trans. Geosci. Remote Sensing*, **28**, 811–816
- Aonashi, K. and Shibata, A. 1996 The impact of assimilating SSM/I precipitable water and rain flag data on humidity analysis and short-term precipitation forecasts. *J. Meteorol. Soc. Japan*, **74**, 77–99
- Barker, D. M., Guo, Y.-R., Huang, W., Xiao, Q. and Bourgeois, A. 2003 'A Three-Dimensional Variational (3D-Var) Data Assimilation System For Use With MM5'. NCAR Technical Notes, NCAR/TN-453+STR, available at <http://www.mmm.ucar.edu/3D-Var/>
- Betts, A. K. 1986 A new convective adjustment scheme. Part I: Observational and theoretical basis. *Q. J. R. Meteorol. Soc.*, **112**, 677–691
- Betts, A. K. and Miller, M. J. 1986 A new convective adjustment scheme. Part II: Single column tests using GATE wave, BOMEX, ATEX and arctic air-mass data sets. *Q. J. R. Meteorol. Soc.*, **112**, 693–709
- Blackadar, A. K. 1979 'High resolution models of the planetary boundary layer'. Pp. 50–85 in *Advances in Environmental Science and Engineering*, **1**, No. 1. Pfafflin and Ziegler, Eds., Gordon and Breach Sci. Publ., New York, USA
- Boutin, J. and Etcheto, J. 1996 Consistency of Geosat, SSM/I, and ERS-1 global surface wind speeds-comparison with in situ data. *J. Atmos. Oceanic Technol.*, **13**, 183–197
- Courtier, P., Thépaut, J.-N. and Hollingsworth, A. 1994 A strategy for operational implementation of 4D-Var using an incremental approach. *Q. J. R. Meteorol. Soc.*, **120**, 1367–1387
- Deblonde, G. 1999 Variational assimilation of SSM/I total precipitable water retrievals in the CMC analysis system. *Mon. Weather Rev.*, **127**, 1458–1476

- Derber, J. C. and Wu, W.-S. 1998 The use of TOVS cloud-cleared radiances in the NCEP SSI analysis system. *Mon. Weather Rev.*, **126**, 2287–2299
- Engelen, R. J. and Stephens, G. L. 1999 Characterization of water-vapour retrievals from TOVS/HIRS and SSM/T-2 measurements. *Q. J. R. Meteorol. Soc.*, **125**, 331–351
- English, S. J., Guillou, C., Prigent, C. and Jones, D. C. 1994 Aircraft measurements of water vapour continuum absorption at millimetre wavelengths. *Q. J. R. Meteorol. Soc.*, **120**, 603–625
- Escoffier, C., Bates, J. J., Chedin, A., Rossow, W. B. and Schmetz, J. 2001 Comparison of upper tropospheric humidity retrievals from TOVS and METEOSAT. *J. Geophys. Res.*, **106**, 5227–5238
- Filiberti, M. A., Eymard, L. and Urban, B. 1994 Assimilation of satellite precipitable water in a meteorological forecast model. *Mon. Weather Rev.*, **122**, 486–506
- Fillion, L. 2002 Variational assimilation of precipitation data and gravity wave excitation. *Mon. Weather Rev.*, **130**, 357–371
- Gérard, É. and Saunders, R. W. 1999 Four-dimensional variational assimilation of Special Sensor Microwave/Imager total column water vapour in the ECMWF model. *Q. J. R. Meteorol. Soc.*, **125**, 3077–3101
- Grell, G. A., Dudhia, J. and Stauffer, D. R. 1994 'A description of the fifth-generation Penn State/NCAR meso-scale model (MM5)'. NCAR/TN-398+STR, National Center for Atmospheric Research, Boulder, CO, USA
- Hollinger, J. 1989 'DMSP special sensor microwave/imager calibration/validation'. Naval Research Laboratory. Final report, Volume 1. Washington, D.C., USA
- Hou, A. Y., Ledvina, D. V., da Silva, M. A., Arlindo, M., Zhang, S. Q., Joiner, J., Atlas, R. M., Huffman, G. J. and Kummerow, C. D. 2000 Assimilation of SSM/I-derived surface rainfall and total precipitable water for improving the GEOS analysis for climate studies. *Mon. Weather Rev.*, **128**, 509–537
- Janjic, Z. I. 1994 The step-mountain Eta coordinate model: further developments of the convection, viscous sublayer and turbulence closure schemes. *Mon. Weather Rev.*, **122**, 927–945
- Joiner, J. and Dee, D. P. 2000 An error analysis of radiance and suboptimal retrieval assimilation. *Q. J. R. Meteorol. Soc.*, **126**, 1495–1514
- Joiner, J. and Rokke, L. 2000 Variational cloud-clearing with TOVS data. *Q. J. R. Meteorol. Soc.*, **126**, 725–748
- Ledvina, D. V. and Pfaendtner, J. 1995 Inclusion of SSM/I total precipitable water estimates into the GOES-1 data assimilation system. *Mon. Weather Rev.*, **123**, 3003–3015
- Liu, D. C. and Nocedal, J. 1989 On the limited memory BFGS method for large scale optimization. *Mathematical Programming*, **45**, 503–528
- Lorenc, A. 1992 Iterative analysis using covariance functions and filters. *Q. J. R. Meteorol. Soc.*, **118**, 569–591
- Lorenc, A. C., Ballard, S. P., Bell, R. S., Ingleby, N. B., Andrews, P. L. F., Barker, D. M., Bray, J. R., Clayton, A. M., Dalby, T., Li, D., Payne, T. J. and Saunders, F. W. 2000 The Met. Office global three-dimensional variational data assimilation scheme. *Q. J. R. Meteorol. Soc.*, **126**, 2991–3012
- MacDonald, A. E., Xie, Y. and Ware, R. H. 2002 Diagnosis of three-dimensional water vapor using a GPS network. *Mon. Weather Rev.*, **130**, 386–397
- McNally, A. P. and Vesperini, M. 1996 Variational analysis of humidity information from TOVS radiances. *Q. J. R. Meteorol. Soc.*, **122**, 1521–1544
- Mo, T. 1999 AMSU-A antenna pattern corrections. *IEEE Trans. Geosci. Rem. Sens.*, **37**, 103–112
- NCEP 1997 Preliminary report <http://www.nhc.noaa.gov/1997danny.html>
- Petty, G. W. 1990 'On the response of the Special Sensor Microwave/Imager to the marine environment—implications for atmospheric parameter retrievals'. Ph.D. Dissertation, University of Washington, USA
- 1994 Physical retrievals of over-ocean rain rate from multichannel microwave imagery. Part II: Algorithm implementation. *Meteorol. Atmos. Phys.*, **54**, 101–122
- Petty, G. W. and Katsaros, K. B. 1992 The response of the SSM/I to the marine environment. Part I: An analytic model for the atmospheric component of observed brightness temperatures. *J. Atmos. Ocean. Tech.*, **9**, 746–761

- Petty, G. W. and Katsaros, K. B. 1994 The response of the SSM/I to the marine environment. Part II: A parameterization of the effect of the sea surface slope distribution on emission and reflection. *J. Atmos. Ocean. Tech.*, **11**, 617–628
- Phalippou, L. 1996 Variational retrieval of humidity profile, wind speed and cloud liquid-water path with the SSM/I: Potential for numerical weather prediction. *Q. J. R. Meteorol. Soc.*, **122**, 327–355
- Pu, Z.-X. and Braun, S. A. 2001 Evaluation of bogus vortex techniques with four-dimensional variational data assimilation. *Mon. Weather Rev.*, **129**, 2023–2039
- Rodgers, C. D. 1990 Characterization and error analysis of profiles retrieved from remote sounding measurements. *J. Geophys. Res.*, **95**, 5587–5595
- Rosenkranz, P. W. 2001 Retrieval of temperature and moisture profiles from AMSU-A and AMSU-B measurements. *IEEE Trans. Geosci. Remote Sensing*, **39**, 2429–2435
- Thépaut, J.-N., Courtier, P., Belaud, G. and Lemaître, G. 1996 Dynamical structure functions in a four-dimensional variational assimilation: A case study. *Q. J. R. Meteorol. Soc.*, **122**, 535–561
- Vesperini, M. 1998 Humidity in the ECMWF model: Monitoring of operational analyses and forecasts using SSM/I observations. *Q. J. R. Meteorol. Soc.*, **124**, 1313–1327
- Wentz, F. J. 1992 Measurement of oceanic wind vector using satellite microwave radiometers. *IEEE Trans. Geosci. Remote Sensing*, **30**, 960–972
- 1993 'User's manual SSM/I antenna temperature tapes revision 2'. RSS technical report 120193, Dec. 1, 1993, Remote Sensing Systems, Santa Rosa, CA, USA
- Wick, G. A., Bates, J. J. and Gottschall, C. C. 2000 Observational evidence of a wind direction signal in SSM/I passive microwave data. *IEEE Trans. Geosci. Remote Sensing*, **38**, 823–837
- Wu, W.-S. and Derber, J. C. 1994 'Inclusion of SSM/I precipitable water observations in the NMC spectral statistical-interpolation analysis system'. Pp. 190–191 in Preprints, *10th Conf. On Numerical Weather Prediction*, Portland, OR, USA. Amer. Meteorol. Soc.
- Xiao, Q., Zou, X. and Kuo, Y.-H. 2000 Incorporating the SSM/I-derived precipitable water and rainfall rate into a numerical model: A case study for the ERICA IOP-4 cyclone. *Mon. Weather Rev.*, **128**, 87–108
- Yu, T.-W., Iredell, M. and Keyser, D. 1997 Global data assimilation and forecast experiments using SSM/I wind speed data derived from neural network algorithm. *Weather and Forecasting*, **12**, 859–865
- Zupanski, M., Zupanski, D., Parrish, D. F., Rogers, E. and DiMego, G. 2002 Four-dimensional variational data assimilation for the blizzard of 2000. *Mon. Weather Rev.*, **130**, 1967–1988